Published in final edited form as:
J Control Release. 2012 February 28; 158(1): 85–92. doi:10.1016/j.jconrel.2011.10.018.

Fluorescent Penetration Enhancers for Transdermal Applications

Jennifer E. Seto[1,a], **Baris E. Polat**[1,a], **Brett VanVeller**[b], **Renata F.V. Lopez**[2,a], **Robert Langer**[a,*], and **Daniel Blankschtein**[a,*]

[a]Department of Chemical Engineering, Massachusetts Institute of Technology, Cambridge, MA 02139, USA

[b]Department of Chemistry, Massachusetts Institute of Technology, Cambridge, MA 02139, USA

Abstract

Chemical penetration enhancers are often used to enhance transdermal drug delivery. However, the fundamental mechanisms that govern the interactions between penetration enhancers and skin are not fully understood. Therefore, the goal of this work was to identify *naturally fluorescent* penetration enhancers (FPEs) in order to utilize well-established fluorescence techniques to directly study the behavior of FPEs within skin. In this study, 12 fluorescent molecules with amphiphilic characteristics were evaluated as skin penetration enhancers. Eight of the molecules exhibited significant activity as skin penetration enhancers, determined using skin current enhancement ratios. In addition, to illustrate the novel, direct, and non-invasive visualization of the behavior of FPEs within skin, three case studies involving the use of two-photon fluorescence microscopy (TPM) are presented, including visualizing glycerol-mitigated and ultrasound-enhanced FPE skin penetration. Previous TPM studies have *indirectly* visualized the effect of penetration enhancers on skin by using a fluorescent dye to probe the transdermal pathways of the enhancer. These effects can now be *directly* visualized and investigated using FPEs. Finally, future studies are proposed for generating FPE design principles. The combination of FPEs with fluorescence techniques represents a useful novel approach for obtaining physical insights on the behavior of penetration enhancers within skin.

Keywords

Skin permeation enhancer; transdermal drug delivery; lipid membrane fluorescent probe; fluorescent amphiphiles; surface-active fluorescent dyes; two-photon fluorescence microscopy

[*]Corresponding authors: Professor Daniel Blankschtein, Massachusetts Institute of Technology, 77 Massachusetts Avenue, Room 66-444, Cambridge, MA 02139, USA, Tel: +1 617 253 4594, Fax: +1 617 252 1651, dblank@mit.edu. Professor Robert Langer, Massachusetts Institute of Technology, 77 Massachusetts Avenue, Room 76-661, Cambridge, MA 02139, USA, Tel: +1 617 253 3107, Fax: +1 617 258 8827, rlanger@mit.edu.
[1]These authors contributed equally to this work.
[2]Present address: Department of Pharmaceutical Sciences, School of Pharmaceutical Sciences of Ribeirão Preto, University of São Paulo, Ribeirão Preto, SP 14040-903, Brazil.

1. Introduction

Chemical penetration enhancers (referred to hereafter as penetration enhancers) are molecules that facilitate drug delivery through a biological membrane. These membranes are often composed of lipid assemblies, including the stratum corneum of the skin, epithelial membranes (e.g. corneal, buccal, and intestinal), and cellular membranes. Many molecules have been identified that can enhance drug delivery [1–5], particularly amphiphiles, which are molecules that contain polar moieties ("head" groups) and non-polar moieties ("tail" groups). Unfortunately, potent penetration enhancers are often also potent irritants [4]. Several investigations have been carried out to elucidate the molecular mechanisms involved in penetration enhancement and in membrane irritation (primarily regarding transdermal drug delivery [1, 4, 5], the focus of this paper). For example, proposed transdermal enhancement mechanisms include extraction or fluidization of lipid bilayers, formation of segregated phases within the bilayers, and others [1]. However, the mechanisms of enhancement and of irritation are still not fully understood. Accordingly, the development of new approaches to evaluate the interactions between penetration enhancers and biological membranes would significantly contribute to a better understanding of the mechanisms involved. In turn, this would aid in the design of potent, yet safer, penetration enhancers for drug delivery.

In the life sciences, the generalized problem of studying the behavior of molecules within biological tissues has often made use of fluorescence-based techniques. Using techniques such as fluorescence resonance energy transfer (FRET), time-resolved fluorescence (TRF), fluorescence polarization (FP), fluorescence recovery after photobleaching (FRAP), fluorescence correlation spectroscopy (FCS), fluorescence lifetime imaging microscopy (FLIM), and confocal and multi-photon fluorescence microscopy, one can study structure, function, and interactions of molecules in biological systems [6]. These well-established techniques require that the molecules of interest be either naturally fluorescent or fluorescently-labeled.

To the best of our knowledge, penetration enhancers have never been synthetically modified with a fluorescent label, presumably because it is believed that the relatively large size of fluorescent labels (generally containing conjugated double bonds) would significantly affect the activity of the enhancers. Therefore, the goal of this work was to identify *naturally fluorescent* penetration enhancers (FPEs) in order to utilize fluorescence techniques to directly study the behavior of FPEs within skin for the first time.

In this study, 12 FPE candidates with amphiphilic characteristics (see Section 2.1) were selected and screened for skin penetration enhancer activity. Subsequently, two-photon fluorescence microscopy (TPM) was used to *directly visualize* and compare the skin penetration profiles of a significant and an insignificant penetration enhancer. In addition, TPM was used to demonstrate that new insights can be obtained by directly visualizing the behavior of FPEs within skin. In transdermal applications, penetration enhancers are often part of a multi-component skin treatment or topical formulation that is designed to overcome the skin barrier in a safe and effective manner. Our findings demonstrate that FPEs may now be used to directly visualize the effect of skin treatments on FPE penetration into skin. This paper presents the first direct visualization of passive, glycerol-mitigated, and ultrasound-assisted FPE penetration into skin. The glycerol and ultrasound treatments are well-established skin treatments that are utilized for decreasing and increasing skin penetration, respectively. Glycerol, a well-known skin moisturizer (humectant), is often used in cosmetic formulations in combination with irritating substances (e.g. surfactants) in order to mitigate skin irritation [7]. On the other hand, low-frequency ultrasound is a physical skin penetration enhancer that is often combined with chemical enhancers, resulting in synergism in

enhancing transdermal drug delivery [8–10]. TPM has previously been used to study the effect of these two skin treatments on penetration enhancers by treating skin either simultaneously or successively with a penetration enhancer and a fluorescent dye in order to *indirectly* visualize the effects of the penetration enhancer on the skin [11–13]. Similarly, dual-channel TPM (which allows for the simultaneous imaging of an exogenous fluorescent probe and the intrinsic skin fluorophores [14]) has previously been used to delineate penetration enhancer-induced changes in permeant diffusion with respect to the skin structural features [12–14]. These effects can now be *directly* visualized and investigated using FPEs.

2. Materials and Methods

2.1 Selection of FPE Candidates

Many potent penetration enhancers are amphiphiles [1–5]. Therefore, 12 molecules that have amphiphilic characteristics were selected as FPE candidates. Fluorescent molecules with various head group chemistries, tail group lengths, and fluorophores were selected as FPE candidates. A list of these 12 molecules is provided in Table 1, and the corresponding chemical structures are shown in Figure 1. Molecules 1 – 4 were selected because they are fluorescent and exhibit the following additional desirable features which are favorable for penetration enhancers: (i) long, saturated, unbranched hydrocarbon chains (or tail groups) [15], and (ii) low molecular weight (less than 500 Daltons) [16]. Molecule 5 was selected because it is one of a handful of fluorescent dyes that is marketed as an amphiphile; this one was selected because of its relatively low molecular weight among amphiphilic dyes. Molecule 6 was selected because it is fluorescent, has a low molecular weight, and was determined to be surface-active in our preliminary experiments (using the procedure described in Section S7.1, molecule 6 lowered the oil/water interfacial tension by 2.8 ± 0.5 mN/m (95% confidence interval)).

Molecules 7 – 12 are all rhodamine derivatives. The selection of these molecules was inspired by recent findings by Polat *et al.* regarding the amphiphilic nature of the fluorescent dye, sulforhodamine B (SRB) [17]. SRB has repeatedly been utilized as a hydrophilic dye. However, SRB is actually an amphiphile, despite being a bulky molecule. SRB was shown to act as a penetration enhancer when combined with a low-frequency ultrasound skin treatment [17] (low-frequency ultrasound is a physical skin penetration enhancer [8, 9]). However, in preliminary passive experiments (without ultrasound), SRB was determined to be an insignificant penetration enhancer (as will be shown in Section 3.1). It was hypothesized that without ultrasound, SRB is too bulky to penetrate into skin in significant amounts, and that smaller rhodamine derivatives may better penetrate into skin and may be mischaracterized in the literature as hydrophilic instead of amphiphilic (as was the case with SRB). Therefore, several rhodamine derivatives whose molecular weights are smaller than that of SRB were selected as FPE candidates.

2.2 Sources of FPE Candidates

Acridine orange 10-nonyl bromide (AO), methyl orange sodium salt (MO), rhodamine 110 chloride (R110), rhodamine B chloride (RB), and SRB sodium salt were obtained from Sigma-Aldrich (St. Louis, MO). 5-dodecanoylaminofluorescein (FLUOR), BODIPY® 500/510 C_8, C_5 (BODIPY1), and BODIPY® FL C_{11} (BODIPY2) were obtained from Invitrogen (Carlsbad, CA). Rhodamine 6G chloride (R6G) was obtained from Acros Organics (Geel, Belgium). Sulforhodamine G sodium salt (SRG) was obtained from Biotium (Hayward, CA). 5-carboxytetramethylrhodamine (TAMRA) was obtained from ChemPep (Wellington, FL). 2-{3-Cyano-4-[4-(dodecyl-methyl-amino)-phenyl]-5,5-dimethyl-5*H*-furan-2-ylidene}-malononitrile (DCDHF) was a gift, synthesized at Kent State University.

MO, RB, and SRG were purified via Büchner funnel vacuum filtration in order to remove water-soluble impurities prior to use (see Section S1 for details). All the other FPE candidates were used as received.

2.3 Sources of General Chemicals

Phosphate buffered saline (PBS) tablets, 1-octanol, and sodium lauryl sulfate (SLS) were obtained from Sigma-Aldrich (St. Louis, MO). PBS was prepared from PBS tablets according to the manufacturer's instructions. Glycerol was obtained from Mallinckrodt Baker (Paris, KY). 200-proof ethanol was obtained from EMD Chemicals (Gibbstown, NJ). Deionized water dispensed from a Milli-Q academic water purification system (Millipore, Bedford, MA) was used to prepare all solutions. All general chemicals were used as received.

2.4 General Protocol for Diffusion Experiments

The following methods have been described previously [18]. Briefly, pig skin was obtained from E.M. Parsons & Sons (Hadley, MA) according to a protocol which was approved by the Committee on Animal Care at MIT. Human cadaver skin was obtained from National Disease Research Interchange (Philadelphia, PA). Skin samples were prepared to a thickness of 700 μm and then mounted into Franz diffusion cells (PermeGear, Hellertown, PA) consisting of a donor chamber and a receiver chamber. Any skin sample having an initial electrical resistivity of <50 kΩ cm^2 (measured with PBS in both chambers) was considered damaged and was discarded.

Subsequently, for all the 24-hour diffusion experiments described below, the PBS solution in the donor chamber was exchanged for 40:60 (by volume) ethanol:PBS (referred to hereafter as 40% ethanol) containing the specified solute concentration. Note that 40% ethanol was used in order to solubilize all the FPE candidates. The donor chamber was sealed using parafilm, and the diffusion cell was covered with aluminum foil to minimize photobleaching. Experiments were conducted at room temperature (25°C).

2.5 Evaluating the Penetration Enhancer Activity of the FPE Candidates

The penetration enhancer activity of the FPE candidates was quantified by the skin current enhancement ratio (ER), based on previous methods for screening penetration enhancers [4, 5, 19, 20]. 1 mM FPE candidate solutions were applied to pig skin (for DCDHF, 0.02 mM was used due to low solubility). Note that 1 mM was chosen to solubilize most FPE candidates in 40% ethanol. Because this was a low concentration compared to the typical ~1% used in previous studies (e.g. [4]), the typical sample size of 3 was insufficient to evaluate penetration enhancer activity at the 95% confidence level. Therefore, the sample size was increased to 9 – 13. Initial skin currents were measured 10 – 15 minutes after the start of the experiment in order to obtain stable current measurements [20]. Final skin currents were measured after 24 hours. The ER is defined as the ratio of the final to the initial skin currents. Both currents were measured through the 40% ethanol solution present in the donor chamber. 40% ethanol was used as the negative control[3]. 2 – 3 negative control samples were included in each day of experiments, resulting in the accumulation of 40 replicates. 1 mM SLS was utilized as a positive control to provide a benchmark ER exhibited by a well-known potent penetration enhancer under these experimental conditions.

[3]It was observed that the negative control ERs exhibited by pig skin harvested in November and December were significantly greater than those reported in this paper (which were measured using pig skin harvested in earlier months in the year). This may be explained due to seasonal variation in skin permeability [21–23]. Therefore, only pig skin batches that yielded low negative control ERs were utilized in this study (i.e. skin from November–December were not used), so that the penetration enhancement induced by the 40% ethanol would not mask the enhancement induced by the FPE candidates.

Note that the experiments described herein were designed to compare each FPE candidate to the negative control, and not to compare potencies among the FPE candidates or to the positive control.

2.6 Two-Photon Microscopy (TPM) Case Study Methods

The purpose of these case studies was to use two-photon fluorescence microscopy (TPM) to demonstrate several applications where the direct visualization of FPEs within skin can provide new physical insight, which is a significant advancement over previous indirect methods (see Section 1). Specifically, the following applications are demonstrated: (I) comparison of the skin penetration profiles of a significant and an insignificant penetration enhancer, (II) visualization of the effect of skin treatments on increasing and decreasing skin penetration, and (III) simultaneous imaging of a FPE and the skin structure.

First, a rationale is provided for selecting which FPE candidate should be used to demonstrate applications I – III. As will be shown in Section 3.1, SRG exhibited significant activity as a penetration enhancer. Since the chemical structure of SRG (see Figure 1) is similar to that of SRB, which did not exhibit significant activity as a penetration enhancer, TPM was used to independently substantiate the interesting findings involving SRG and SRB (application I). Subsequently, SRG became a convenient choice to demonstrate glycerol-mitigated and ultrasound-assisted FPE skin penetration (application II) because baseline images of SRG skin penetration were already obtained for application I. Finally, SRG fluorescence could be filtered from that of the skin for dual-channel imaging (application III).

2.6.1 Preparation of Skin Samples for TPM Imaging—For SRB-treated skin (application I), 1 mM SRB was applied to pig skin for 24 hours. For SRG-treated skin (applications I and II), 1 mM SRG was applied to pig skin for 24 hours. For skin treated with SRG and glycerol (application II), the donor solution was prepared as follows: (1) glycerol was added to 40% ethanol to attain 10 wt% glycerol (5–15 wt% glycerol is commonly used in studies on the role of glycerol in cosmetic and pharmaceutical formulations [24]), and (2) SRG was subsequently added to attain 1 mM SRG. For skin treated with SRG and ultrasound (application II): ultrasound, with the solid probe tip immersed in a coupling medium containing 1 mM SRG in 40% ethanol, was applied to pig skin with a VCX 130 (Sonics & Materials, Newtown, CT) at the following ultrasound parameters [25]: frequency - 40 kHz, intensity - 7.3 W/cm^2 (for a coupling medium of 40% ethanol, this corresponds to a 40% amplitude setting, as verified using calorimetry), pulsing - 5 seconds on, 5 seconds off, tip displacement - 3 mm. The coupling medium was replaced at least every 30 seconds (“on” time) to reduce thermal effects. Ultrasound was applied to the skin until red patches (corresponding to localized regions [26] of SRG penetration) were visible on the skin surface (requiring 2 minutes of “on” time, which is typical for treatments involving ultrasound and a chemical enhancer [9, 10]), thus indicating that SRG had penetrated into the skin in sufficient amounts for imaging.

For dual-channel TPM imaging (application III), 2 μg/mL (3.6 μM) SRG was applied to human skin for 24 hours. The dilution of SRG (compared with 1 mM for applications I and II) reduces the SRG fluorescence signal such that it is comparable with that of the skin, which enables the detection of both signals. Note that dual-channel imaging with pig skin was unsuccessful (data not shown) because pig skin fluoresces more intensely in the red region than human skin [27]. As a result, pig skin and SRG fluorescence signals could not be separated.

Immediately following the end of each skin treatment, the skin surface was rinsed with 40% ethanol and blotted with a Kimwipe to remove excess solute. The treated skin area was

isolated using scissors and inserted into an imaging chamber (Coverwell PCI-A-0.5, Grace Bio-Labs, Bend, OR) with PBS as the mounting medium. The imaging chamber was sealed with a No. 1.5 glass coverslip.

2.6.2 TPM Imaging—Images were obtained on a Zeiss LSM 510 microscope using a 63x oil objective and a Spectra-Physics Mai Tai laser tuned to 780 nm. TPM imaging was conducted based on previously published methods [13, 14, 28]. The following settings were used for the three TPM applications: (a) for SRB-, SRG-, and SRG/glycerol-treated pig skin, the laser power was measured at the sample to be 0.4 mW. Emission wavelengths ≤ 685 nm were collected. Configurations were set such that in the absence of fluorophores, no signal was detected, (b) for SRG/ultrasound-treated pig skin, the laser power was 0.7 mW for imaging 0–20 μm below the skin surface and 5 mW for imaging depths > 20 μm. Emission wavelengths in the range of 565 – 615 nm were collected. Configurations were set such that in the absence of SRG, no signal was detected, and (c) for dual-channel imaging of SRG and human skin autofluorescence, the laser power was 34 mW. In the "green" channel, emission wavelengths < 515 nm were collected (corresponding to skin autofluorescence [29]). In the "red" channel, emission wavelengths in the range of 565 – 615 nm were collected (corresponding to SRG fluorescence; note that the SRG emission peaks at 548 nm, but the collection of longer wavelengths minimized the overlap with the skin autofluorescence). Using the stated experimental conditions and microscopy configurations, the skin autofluorescence intensities in the presence and in the absence of SRG were found to be comparable, thus verifying that SRG did not introduce noise in the green channel. Configurations were set such that in the absence of SRG, no signal was detected in the red channel (see Figure S1).

Up to six 200 μm × 200 μm sites were imaged within each skin sample. Images were obtained in the plane parallel to the skin surface (xy-mode), and optical sections were made in the z-stack mode (e.g. see Figure S2). In all the figures presented, a red color scheme is utilized to illustrate routes of FPE penetration. It is important to recognize that the images serve to provide *qualitative* information regarding the visualization of FPE penetration patterns.

2.6.3 Image Analysis—Images were analyzed using ImageJ software (National Institutes of Health, Bethesda, MD). The "Plot Z-axis profile" function was used to calculate the average fluorescence intensity vs. skin penetration depth from each series of images obtained in the z-stack mode (e.g. Figure S2). These data were averaged over all of the sites imaged for each skin treatment. In addition, for all figures, the brightness and contrast of the images was adjusted first by using the "Auto" feature in order to enhance the visibility of the regions of FPE penetration, and second by increasing the minimum displayed pixel value. These adjustments were propagated to control images to ensure that the control images remained black.

It is important to recognize that SRB fluoresces more brightly than SRG in non-polar environments. Therefore, in order to compare the penetration of SRB and SRG into skin, the SRB fluorescence intensities were normalized by the ratio of the SRB and SRG fluorescence intensities within PBS-saturated octanol (see Section S4 for details).

2.7 Statistical Analysis

Two-sample, two-tailed *t*-tests assuming unequal variances were used to compare skin current ERs, fluorescence intensities, and oil/water interfacial tension values. In all analyses, p values < 0.05 were considered to be statistically significant.

3. Results and Discussion

3.1 Identification of Fluorescent Penetration Enhancers

The activity of the FPE candidates as skin penetration enhancers was quantified by skin current enhancement ratio (ER). The results of these experiments are summarized in Figure 2. Eight of the twelve FPE candidates (BODIPY1, AO, SRG, RB, R6G, DCDHF, MO, and BODIPY2) exhibited ERs significantly different from that of the negative control; therefore, they are transdermal FPEs. These results demonstrate that the presence of a fluorescent group in the structure does not prevent molecules from acting as skin penetration enhancers.

Next, several comments can be made regarding the chemical structures of the FPEs. First, the rhodamine candidates (molecules 7 – 12 in Table 1) are generally bulkier than the candidates with long, saturated carbon chains (molecules 1 – 5 in Table 1). Based on this comparison, one would intuitively expect the candidates with long carbon chains to better penetrate into skin and perturb the skin lipid bilayers. Nevertheless, the ERs of these candidates and of the rhodamine candidates are evenly interspersed between the ERs of the positive and negative controls. These results are in agreement with previous findings. Recall that many drugs that are successfully administered via a transdermal patch are hormones with multiple rings [30], similar to the rhodamine candidates. In addition, Mitragotri and co-workers previously designed over 300 mutated chemical skin penetration enhancers based on potency and safety [4]. Their 6 best compounds were ones with either long, saturated carbon chains or with multiple rings.

Second, it is interesting that DCDHF, while applied to skin at $1/50^{th}$ of the concentration of the other candidates, still exhibited a significantly large ER. This indicates that this structure has great potential as a FPE. There are three distinguishing features of DCDHF that may contribute to its significant penetration enhancer activity: (i) nitrile head groups, which have been linked with skin irritation and toxicity [31] (and these properties are often exhibited by potent penetration enhancers [4]), (ii) a 12-carbon tail, which has previously been shown to be the optimal tail length for skin penetration enhancers [15], and (iii) a compact fluorophore with a small number of rings, located adjacent to the nitrile head groups. However, in spite of the fact that DCDHF exhibited potency at a low concentration, it is limited by its poor water solubility. This structure, which has been shown to be readily derivatized [32, 33], may be improved by adding a water-soluble group such as sulfonic acid (e.g. fluorophore 21 in [33], shown in Figure S5).

Third, in spite of the fact that SRG and SRB have similar chemical structures, SRG is a significant FPE, while SRB is not. Furthermore, there is a significant difference between the ERs of SRG and SRB, which was an unexpected but opportune finding based on our experimental design (see Section 2.5). In Section 3.2.2, TPM was utilized to visualize the skin penetration profiles of SRG and SRB in order to independently substantiate these interesting results with data from image analyses. As discussed in Section 2.1, SRG was selected as a FPE candidate because it is smaller than SRB. However, over the range of molecular weights studied (327 – 581 Daltons), there is no correlation between molecular weight and potency as a transdermal FPE (see Section S6). One difference in their chemical structures that may contribute to their difference in skin penetration enhancer activities is that the 3-ring xanthene structure of SRB has a delocalized charge of +1 due to resonance; the xanthene structure of SRG is not necessarily protonated. Therefore, the structure of SRG allows for a better distribution of charges and a clearer distinction between head and tail regions (in fact, SRG is more amphiphilic than SRB; see Section S7). In addition, the +1 charge of the xanthene structure of SRB may result in different interactions with the negatively-charged skin, intramolecular interactions with the sulfonate-containing pendant group, or a higher degree of hydrophilicity. It would be interesting to investigate the

structure-activity differences (i.e. the relationship between the chemical structure and the penetration enhancer activity [34–36]) between SRG and SRB in future studies. Note that ionization and hydrophilicity have previously been shown to affect penetration enhancer activity [19, 37].

3.2 TPM Case Studies: Visualization of FPE Penetration into Skin

In the previous section, eight FPE candidates were demonstrated to be skin penetration enhancers. These FPEs now enable the use of a multitude of fluorescence techniques to investigate FPE-enhanced transdermal applications. As an example, two-photon fluorescence microscopy (TPM) was used to demonstrate several applications where the *direct* visualization of FPEs can provide new physical insight. This is a significant advancement over previous TPM studies that *indirectly* visualized the effect of penetration enhancers on the skin, as discussed in Section 1.

3.2.1 Visualization of the Effect of Skin Treatments on SRG Penetration—

Representative TPM images of SRG-, SRG/glycerol-, and SRG/ultrasound-treated skin samples are shown in Figure 3. Recall that glycerol and ultrasound treatments are well-established skin treatments that are utilized for decreasing and increasing skin penetration, respectively (see Section 1). First, the effect of glycerol on SRG penetration into skin is discussed. In SRG-treated skin, the SRG remained localized within the lipid bilayers surrounding the corneocytes (see Figure 3A); this localization was observed uniformly throughout the skin sample. With the addition of glycerol, the SRG penetration pattern remained the same (see Figure 3B), however, SRG fluorescence intensities were smaller. The images were analyzed to determine the average SRG intensity profiles in the presence and in the absence of glycerol. These data, presented in Figure 4, show that glycerol significantly reduced the intensity of SRG visualized within the skin, which is consistent with the well-documented biological effects of glycerol on the skin [7, 12, 24, 38]. In particular, the data is consistent with a previous report that glycerol reduces the average aqueous pore radius in the stratum corneum, which sterically reduced the ability of SLS (a penetration enhancer with lower molecular weight than SRG) to partition into the skin [24]. Note that it was verified that glycerol does not directly affect the fluorescence intensity of SRG (i.e. the SRG donor solution fluorescence intensities with and without 10% glycerol were the same; data not shown).

Next, the effect of ultrasound on SRG penetration into skin is discussed. Ultrasound significantly affects the SRG penetration pattern. Figure 3C and Figure 3D show that ultrasound assists the penetration of SRG into skin via irregular pathways. The spacing between penetration routes is often less than 20 μm (see the scale bar), indicating that the routes are transcellular. This is consistent with previous reports that ultrasound can create transcellular pathways in the stratum corneum [13, 39]. Furthermore, SRG penetration was only observed in discrete regions that were heterogeneously distributed across the treated skin area, corresponding to localized transport regions (LTRs) that have been well documented within ultrasound-treated skin [8, 9, 26]. LTRs are regions where ultrasound-induced cavitation microjets drive the coupling medium into the skin [8, 25] (see [8] for an illustration of ultrasound's skin penetration enhancement mechanism). Finally, with the assistance of ultrasound, SRG penetrated into the epidermis in localized regions in significant amounts (see Figure 3E), whereas without ultrasound, SRG did not significantly penetrate into the epidermis (not shown). Note that in Figure 3E, the 5-μm circular regions where SRG did not penetrate correspond to the epidermal cell nuclei.

This TPM application demonstrates that by using a FPE, one can directly visualize how changes to a topical formulation or skin treatment affect the partitioning, penetration, and spatial distribution of the FPE within skin. FPEs can now be utilized to aid in designing safe

and effective skin treatments and topical formulations, which often contain penetration enhancers.

3.2.2 Visual Comparison of the Penetration Profiles of SRG and SRB—SRG- and SRB-treated skin samples were imaged using TPM. In both cases, the fluorescence remained localized within the lipid bilayers surrounding the corneocytes (see Figure S3). However, Figure 5 shows that the fluorescence intensity profiles are significantly different. In particular, the SRG surface intensity was significantly higher than that of SRB, suggesting that SRG (which is a FPE; see Section 3.1) partitioned more readily into the skin than SRB (which is not a penetration enhancer; see Section 3.1). With higher resolution fluorescence techniques (such as single-molecule fluorescence techniques [6]), one may be able to elucidate the differences in mechanisms of partitioning and diffusing into skin for significant and insignificant penetration enhancers, which would aid in designing potent, yet safe, penetration enhancers for drug delivery.

3.2.3 Dual-Channel Imaging of SRG and Skin Autofluorescence—Skin autofluorescence stems from intrinsic skin components, including collagen, elastin, aromatic amino acids, and cofactors [40]. These components reside in the lipid bilayers; by imaging skin autofluorescence, one can delineate the corneocyte-lipid bilayer interface. Therefore, by simultaneously imaging the probe spatial distribution and the skin autofluorescence, one can identify changes in probe partitioning between the corneocytes and the lipid bilayers and/or probe-induced structural changes in the skin structure [14, 40].

This is demonstrated using dual-channel TPM to image SRG-treated skin (see Figure 6). In the green channel, the skin autofluorescence is generally limited to the intercellular regions surrounding the corneocytes, thereby delineating the skin structure. The corneocyte dimensions are approximately 20 μm, which is consistent with previous reports [41]. In the red channel, it is clear that SRG is not always present throughout the entire intercellular space; instead, there is an apparent preferential localization within a 1-μm thick region at the corneocyte-lipid interface (see arrows in Figure 6). This region may include the 15-nm cornified cell envelope, which is composed of a mixture of cross-linked protein filaments and lipid molecules [41]. This localization is consistent with the amphiphilic character of SRG, which was evaluated in Section S7. Other higher resolution fluorescence techniques (such as single-molecule fluorescence techniques [6]) can be used to investigate this localization further, which may contribute new physical insights on the *interactions* between FPEs and the skin.

Note that in Figure 3 and Figure 6, SRG was applied to different skin membranes (pig and human, respectively) and at different concentrations (1 mM and 3.6 μM, respectively). These differences may impact the visualization of SRG localization in the corneocyte envelope and in the intercellular lipids. Therefore, we caution the direct comparison of these figures.

3.3 Proposed Studies for Generating FPE Design Principles

Future studies should be conducted to rank the FPEs by penetration enhancer activity. The data reported in the present study could not be used to rank the FPEs because the method described in Section 2.5 yielded a difference in ERs between the positive and negative controls that is statistically significant, but small in magnitude (see Figure 2). This result made it difficult to obtain significantly different ERs between the FPE candidates and SLS. To elucidate the difference in potency between two FPEs, one may: (1) apply them to the skin at higher concentrations to increase the range of ERs, and/or (2) increase the number of

replicates to reduce experimental variability. It would be interesting to conduct this experiment to rank various FPEs and generate FPE design principles.

For example, both BODIPY1 and BODIPY2 are significant FPEs (see Section 3.1), yet we speculate that there may be a difference in their potencies which may lead to an exciting area for future research. While both molecules have long hydrocarbon chains, the fluorophore in BODIPY1 is positioned in the middle of the chain, and the fluorophore in BODIPY2 is positioned at the end of the chain. Penetration enhancers with long hydrocarbon chains can readily intercalate into the structured lipid bilayers of the stratum corneum and disrupt the lipid packing, thereby increasing lipid fluidity and reducing the skin diffusion barrier [42]. However, we hypothesize that the location of the fluorophore at the end of the hydrocarbon chain (as in BODIPY2) would hinder the chain from intercalating into lipid bilayers. Our hypothesis is supported by a previous study which showed that the depth of penetration into a lipid membrane depends on the steric bulk of the intercalant [43]. If BODIPY1 is significantly more potent than BODIPY2, this would suggest that positioning the fluorophore adjacent to the head group, as proposed in Figure S6, may result in a more potent FPE. Note that BODIPY is a popular fluorophore because its robust fluorescence properties are highly favorable for many imaging applications [44]. Therefore, a potent BODIPY-based FPE has the potential to be utilized in many types of imaging studies.

In a second application, SRG is more amphiphilic than SRB, but is less amphiphilic than SLS (see Section S7). It would be interesting to see if this trend is observed when comparing their penetration enhancer activities. To the best of our knowledge, correlations between amphiphilicity and penetration enhancer activity have never been investigated, in spite of the fact that many potent enhancers are amphiphiles [1–5]. We have already (unintentionally, but opportunely) observed a significant difference in the ERs for SRG and SRB (see Section 3.1). The additional experiments described above would be needed to determine if SRG and SLS exhibit significantly different ERs. If SRG exhibits significantly less penetration enhancer activity than SLS, then the evaluation of a correlation between amphiphilicity and penetration enhancer activity would be an exciting area for future study.

4. Conclusions

We have identified eight FPEs for transdermal applications. TPM was utilized to directly and non-invasively visualize FPEs within skin for the first time, including: (i) visualizing glycerol-mitigated and ultrasound-enhanced FPE skin penetration, (ii) visually confirming that SRG and SRB exhibit significantly different fluorescence intensity profiles within the skin, which is consistent with the finding that SRG is a FPE while SRB is not, and (iii) using dual-channel TPM to demonstrate the visualization of a FPE with respect to the skin structure. These demonstrations reinforce the novel strategy of combining FPEs with well-established fluorescence techniques to elucidate mechanisms of penetration enhancement and skin irritation. FPEs will allow a multitude of fluorescence techniques to be utilized in order to directly visualize penetration-enhanced transdermal drug delivery. With further studies, more potent transdermal FPEs may be designed. New physical insights obtained using this approach will aid in designing effective penetration enhancers for transdermal drug delivery applications.

Supplementary Material

Refer to Web version on PubMed Central for supplementary material.

Acknowledgments

We thank Professor R.J. Twieg (Kent State University), Professor W.E. Moerner (Stanford University), and Na Liu (Kent State University) for providing us with DCDHF. We thank Professor D.J. Irvine (MIT) for use of his LSM 510. This research was funded by the National Institutes of Health (Grant# EB-00351) and the U.S. Army Research Office through the Institute for Soldier Nanotechnologies at MIT (Project 2.3.2: Non-Invasive Delivery and Sensing, Grant# DAAD-19-02-D-002). JES was supported in part by a National Science Foundation Graduate Research Fellowship. RFVL was supported by the Brazilian National Council for Scientific and Technological Development (CNPq) and the São Paulo Research Foundation (FAPESP). The contents of this article are solely the responsibility of the authors; no official endorsements by the U.S. Government nor by the Brazilian Government should be inferred.

References

1. Williams AC, Barry BW. Penetration enhancers. Adv. Drug Del. Rev. 2004; 56(5):603–618.
2. Nicolazzo JA, Reed BL, Finnin BC. Buccal penetration enhancers--how do they really work? J. Controlled Release. 2005; 105(1–2):1–15.
3. Sultana Y, Aqil M, Ali A, Samad A. Advances in the topical ocular drug delivery. Expert Rev. Ophthalmol. 2007; 2(2):309–323.
4. Karande P, Jain A, Ergun K, Kispersky V, Mitragotri S. Design principles of chemical penetration enhancers for transdermal drug delivery. Proc. Natl. Acad. Sci. USA. 2005; 102(13):4688–4693. [PubMed: 15774584]
5. Karande P, Jain A, Mitragotri S. Discovery of transdermal penetration enhancers by high-throughput screening. Nat. Biotechnol. 2004; 22(2):192–197. [PubMed: 14704682]
6. Demchenko, AP. Introduction to Fluorescence Sensing. Dordrecht, Netherlands: Springer; 2009.
7. Fluhr JW, Darlenski R, Surber C. Glycerol and the skin: holistic approach to its origin and functions. Br. J. Dermatol. 2008; 159(1):23–34. [PubMed: 18510666]
8. Polat BE, Hart D, Langer R, Blankschtein D. Ultrasound-mediated transdermal drug delivery: Mechanisms, scope, and emerging trends. J. Controlled Release. 2011; 152(3):330–348.
9. Polat BE, Blankschtein D, Langer R. Low-frequency sonophoresis: application to the transdermal delivery of macromolecules and hydrophilic drugs. Expert Opin. Drug Deliv. 2010; 7(12):1415–1432. [PubMed: 21118031]
10. Polat BE, Seto JE, Blankschtein D, Langer R. Application of the aqueous porous pathway model to quantify the effect of sodium lauryl sulfate on ultrasound-induced skin structural perturbation. J. Pharm. Sci. 2011; 100(4):1387–1397.
11. Tezel A, Sens A, Tuchscherer J, Mitragotri S. Synergistic effect of low-frequency ultrasound and surfactants on skin permeability. J. Pharm. Sci. 2002; 91(1):91–100. [PubMed: 11782900]
12. Ghosh S, Kim D, So P, Blankschtein D. Visualization and quantification of skin barrier perturbation induced by surfactant-humectant systems using two-photon fluorescence microscopy. J. Cosmet. Sci. 2008; 59(4):263–289. [PubMed: 18818848]
13. Kushner J, Kim D, So PT, Blankschtein D, Langer RS. Dual-channel two-photon microscopy study of transdermal transport in skin treated with low-frequency ultrasound and a chemical enhancer. J. Invest. Dermatol. 2007; 127(12):2832–2846. [PubMed: 17554365]
14. Yu B, Kim KH, So PTC, Blankschtein D, Langer R. Visualization of oleic acid-induced transdermal diffusion pathways using two-photon fluorescence microscopy. J. Invest. Dermatol. 2003; 120(3):448–455. [PubMed: 12603859]
15. Zatz, JL.; Lee, B. Surfactants in Cosmetics. Rieger, MM.; Rhein, LD., editors. New York, NY: Marcel Dekker; 1997. p. 501-517.
16. Bos JD, Meinardi MMHM. The 500 Dalton rule for the skin penetration of chemical compounds and drugs. Exp. Dermatol. 2000; 9(3):165–169. [PubMed: 10839713]
17. Polat BE, Lin S, Mendenhall JD, VanVeller B, Langer R, Blankschtein D. Experimental and molecular dynamics investigation into the amphiphilic nature of sulforhodamine B. J. Phys. Chem. B. 2011; 115(6):1394–1402. [PubMed: 21222449]

18. Seto JE, Polat BE, Lopez RFV, Blankschtein D, Langer R. Effects of ultrasound and sodium lauryl sulfate on the transdermal delivery of hydrophilic permeants: comparative in vitro studies with full-thickness and split-thickness pig and human skin. J. Controlled Release. 2010; 145(1):26–32.
19. Karande P, Jain A, Mitragotri S. Relationships between skin's electrical impedance and permeability in the presence of chemical enhancers. J. Controlled Release. 2006; 110(2):307–313.
20. Rachakonda VK, Yerramsetty KM, Madihally SV, Robinson RL Jr, Gasem KA. Screening of chemical penetration enhancers for transdermal drug delivery using electrical resistance of skin. Pharm. Res. 2008; 25(11):2697–2704. [PubMed: 18683029]
21. Pitman IH, Rostas SJ, Downes LM. Effects of breed, season, temperature, and solvents on the permeability of frozen and reconstituted cattle skin to levamisole. J. Pharm. Sci. 1983; 72(3):218–221. [PubMed: 6842371]
22. Magerl W, Westerman RA, Mohner B, Handwerker HO. Properties of transdermal histamine iontophoresis: differential effects of season, gender, and body region. J. Invest. Dermatol. 1990; 94(3):347–352. [PubMed: 2307854]
23. Schroder J. Cutaneous absorption of chemicals. J. S. Afr. Vet. Assoc. 1986; 57(3):169–176. [PubMed: 3543356]
24. Ghosh S, Blankschtein D. The role of sodium dodecyl sulfate (SDS) micelles in inducing skin barrier perturbation in the presence of glycerol. J. Cosmet. Sci. 2007; 58(2):109–133. [PubMed: 17520152]
25. Polat BE, Figueroa PL, Blankschtein D, Langer R. Transport pathways and enhancement mechanisms within localized and non-localized transport regions in skin treated with low-frequency sonophoresis and sodium lauryl sulfate. J. Pharm. Sci. 2011; 100(2):512–529. [PubMed: 20740667]
26. Kushner J, Blankschtein D, Langer R. Heterogeneity in skin treated with low-frequency ultrasound. J. Pharm. Sci. 2008; 97(10):4119–4128. [PubMed: 18240305]
27. Drakaki E, Borisova E, Makropoulou M, Avramov L, Serafetinides AA, Angelov I. Laser induced autofluorescence studies of animal skin used in modeling of human cutaneous tissue spectroscopic measurements. Skin Res. Technol. 2007; 13(4):350–359. [PubMed: 17908185]
28. Yu B, Dong C-Y, So PTC, Blankschtein D, Langer R. In vitro visualization and quantification of oleic acid induced changes in transdermal transport using two-photon fluorescence microscopy. J. Invest. Dermatol. 2001; 117(1):16–25. [PubMed: 11442745]
29. Na RH, Stender IM, Ma LX, Wulf HC. Autofluorescence spectrum of skin: component bands and body site variations. Skin Res. Technol. 2000; 6(3):112–117. [PubMed: 11428953]
30. Prausnitz MR, Langer R. Transdermal drug delivery. Nat. Biotechnol. 2008; 26(11):1261–1268. [PubMed: 18997767]
31. Bagley DM, Gardner JR, Holland G, Lewis RW, Regnier JF, Stringer DA, Walker AP. Skin irritation: Reference chemicals data bank. Toxicol. In Vitro. 1996; 10(1):1–6. [PubMed: 20650176]
32. Lord SJ, Conley NR, Lee H-LD, Nishimura SY, Pomerantz AK, Willets KA, Lu Z, Wang H, Liu N, Samuel R, Weber R, Semyonov A, He M, Twieg RJ, Moerner WE. DCDHF fluorophores for single-molecule imaging in cells. ChemPhysChem. 2009; 10(1):55–65. [PubMed: 19025732]
33. Wang H, Lu Z, Lord SJ, Moerner WE, Twieg RJ. Modifications of DCDHF single molecule fluorophores to impart water solubility. Tetrahedron Lett. 2007; 48(19):3471–3474. [PubMed: 19759848]
34. Kanikkannan, N.; Babu, RJ.; Singh, M. Percutaneous Penetration Enhancers. Smith, EW.; Maibach, HI., editors. Boca Raton, FL: CRC Press; 2006. p. 17-33.
35. Kanikkannan N, Kandimalla K, Lamba SS, Singh M. Structure-activity relationship of chemical penetration enhancers in transdermal drug delivery. Curr. Med. Chem. 2000; 7(6):593–608. [PubMed: 10702628]
36. Warner KS, Li SK, He N, Suhonen TM, Chantasart D, Bolikal D, Higuchi WI. Structure-activity relationship for chemical skin permeation enhancers: Probing the chemical microenvironment of the site of action. J. Pharm. Sci. 2003; 92(6):1305–1322. [PubMed: 12761819]

37. Novotny M, Klimentova J, Janusova B, Palat K, Hrabalek A, Vavrova K. Ammonium carbamates as highly active transdermal permeation enhancers with a dual mechanism of action. J. Controlled Release. 2011; 150(2):164–170.

38. Ghosh S, Hornby S, Grove G, Zerwick C, Appa Y, Blankschtein D. Ranking of aqueous surfactant-humectant systems based on an analysis of in vitro and in vivo skin barrier perturbation measurements. J. Cosmet. Sci. 2007; 58(6):599–620. [PubMed: 18305874]

39. Kushner J, Blankschtein D, Langer R. Experimental demonstration of the existence of highly permeable localized transport regions in low-frequency sonophoresis. J. Pharm. Sci. 2004; 93(11): 2733–2745. [PubMed: 15389675]

40. Alvarez-Roman R, Naik A, Kalia YN, Fessi H, Guy RH. Visualization of skin penetration using confocal laser scanning microscopy. Eur. J. Pharm. Biopharm. 2004; 58(2):301–316. [PubMed: 15296957]

41. Walters, KA. Dermatological and Transdermal Formulations. Walters, KA.; Roberts, MS., editors; Vol. Vol. 119. New York: Marcel Dekker, Inc.; 2002. p. 1-39.

42. Golden GM, McKie JE, Potts RO. Role of stratum corneum lipid fluidity in transdermal drug flux. J. Pharm. Sci. 1987; 76(1):25–28. [PubMed: 3585718]

43. Bodner E, Afri M, Frimer AA. Determining radical penetration into membranes using ESR splitting constants. Free Radic. Biol. Med. 2010; 49(3):427–436. [PubMed: 20444432]

44. Benniston AC, Copley G. Lighting the way ahead with boron dipyrromethene (BODIPY) dyes. Phys Chem Chem Phys. 2009; 11(21):4124–4131. [PubMed: 19458813]

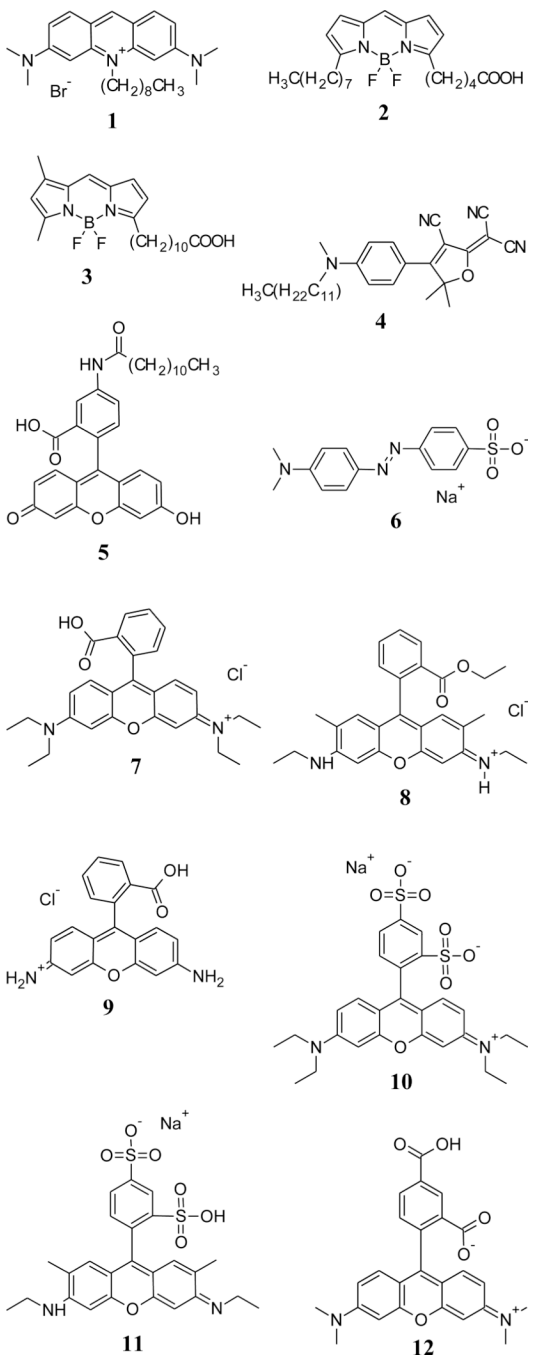

Figure 1.
Chemical structures of the fluorescent penetration enhancer (FPE) candidates.

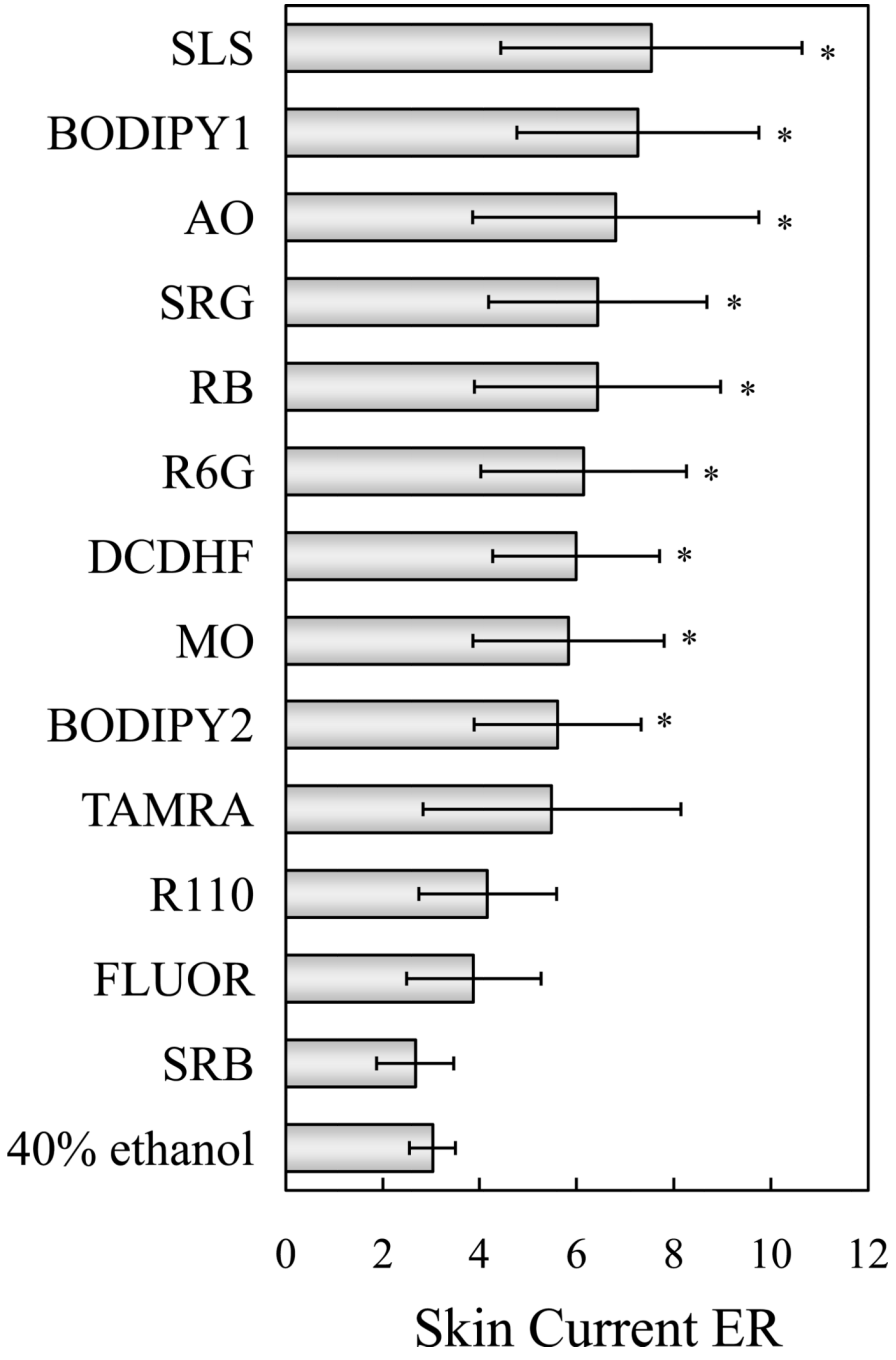

Figure 2.

Skin current enhancement ratios (ERs) exhibited by the FPE candidates considered. SLS served as a positive control. Solute concentrations were 1 mM (except for DCDHF, 0.02 mM). Error bars indicate 95% confidence intervals. * indicates significant difference compared to 40% ethanol (negative control). $n = 40$ for 40% ethanol; $n = 9 – 13$ for all others.

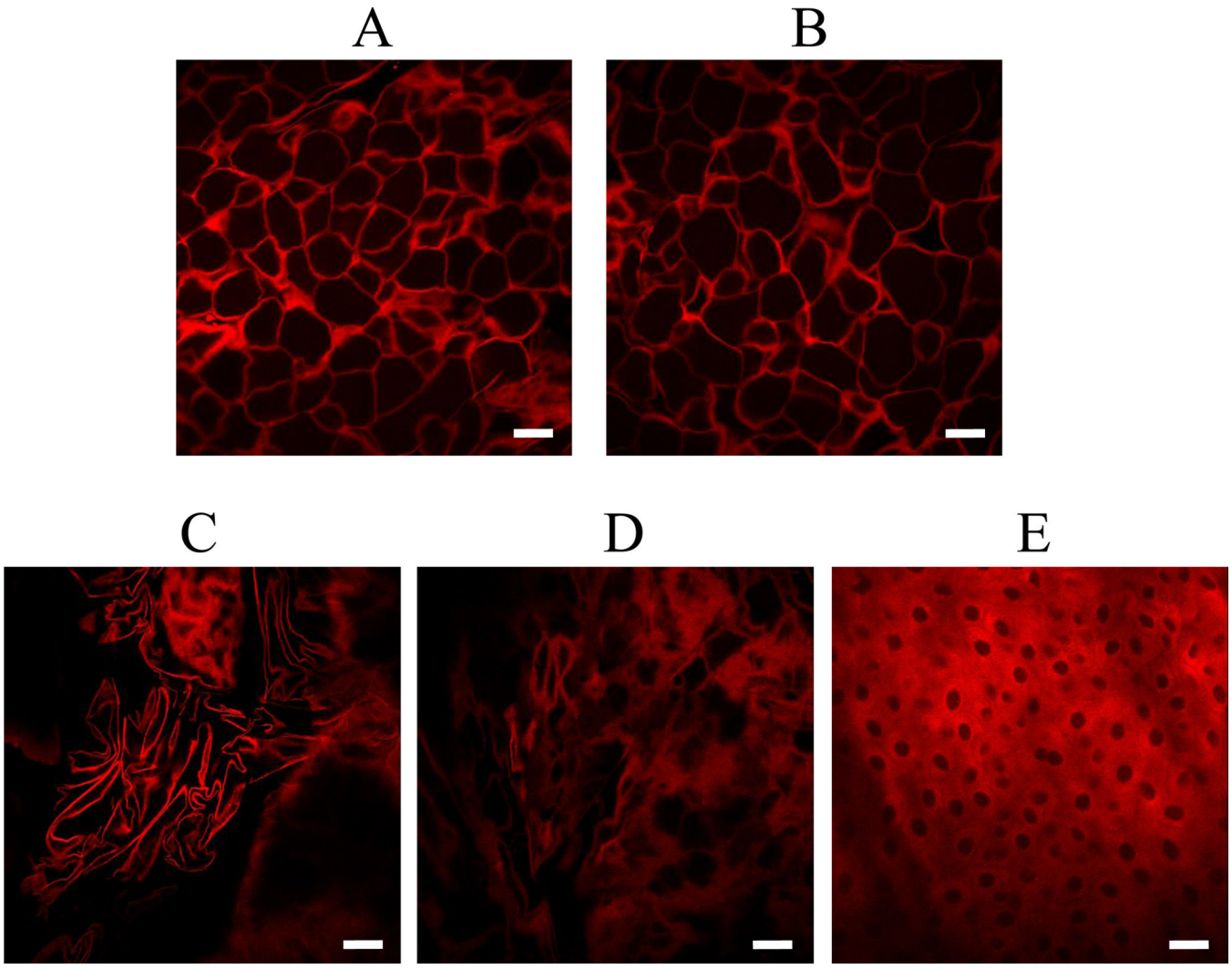

Figure 3.
SRG penetration patterns within SRG-treated, SRG/glycerol-treated, and SRG/ultrasound-treated pig skin. The presence of SRG is indicated by the red color. (A) Representative image of SRG-treated skin (image depth, 2 μm below the skin surface). (B) Representative image of SRG/glycerol-treated skin (depth, 2 μm). (C, D) Selected regions of interest within the stratum corneum of SRG/ultrasound-treated skin (depth, 2 μm). (E) Selected region of interest within the epidermis of SRG/ultrasound-treated skin (depth, 34 μm). Bar = 20 μm.

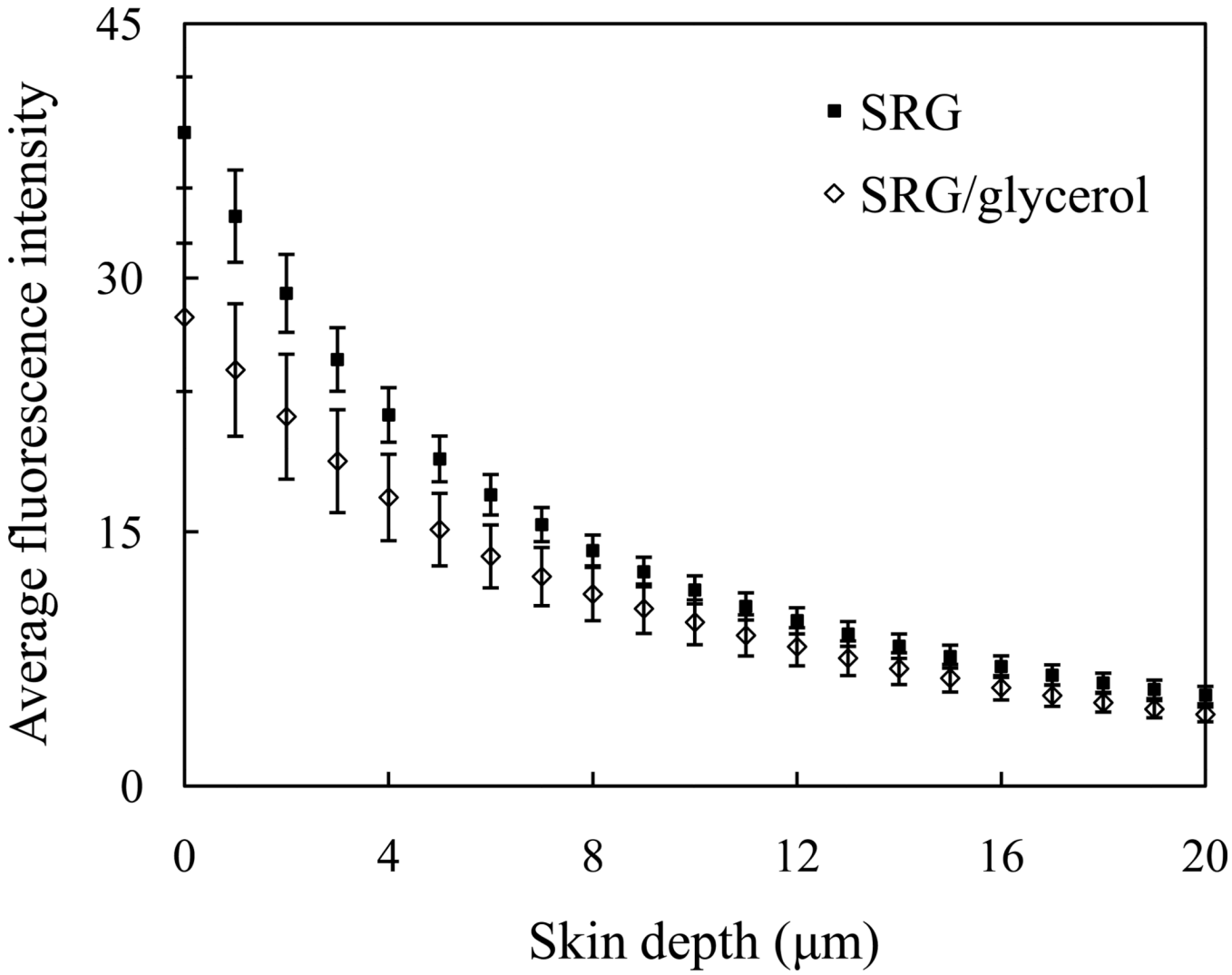

Figure 4.

Average SRG fluorescence intensity as a function of skin depth, in the presence and in the absence of 10% glycerol. Fluorescence intensities are significantly different at all skin depths. Error bars indicate 95% confidence intervals. *n* = 18 sites for SRG; *n* = 12 sites for SRG/glycerol.

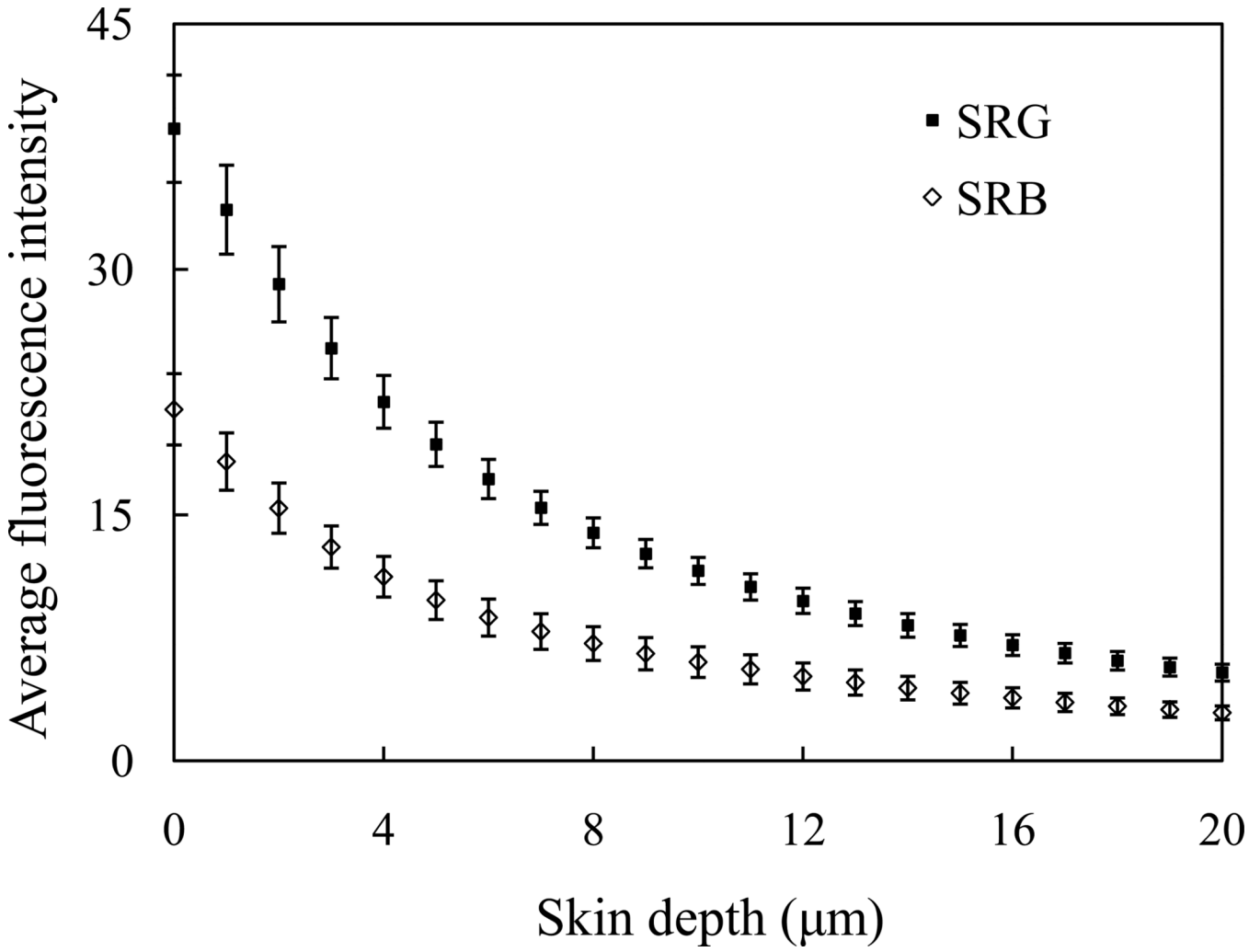

Figure 5.
Average SRG and SRB fluorescence intensity as a function of skin depth. Fluorescence intensities are significantly different at all skin depths. Error bars indicate 95% confidence intervals. *n* = 18 sites for both SRG and SRB. SRB data were normalized as described in Section 2.6.3.

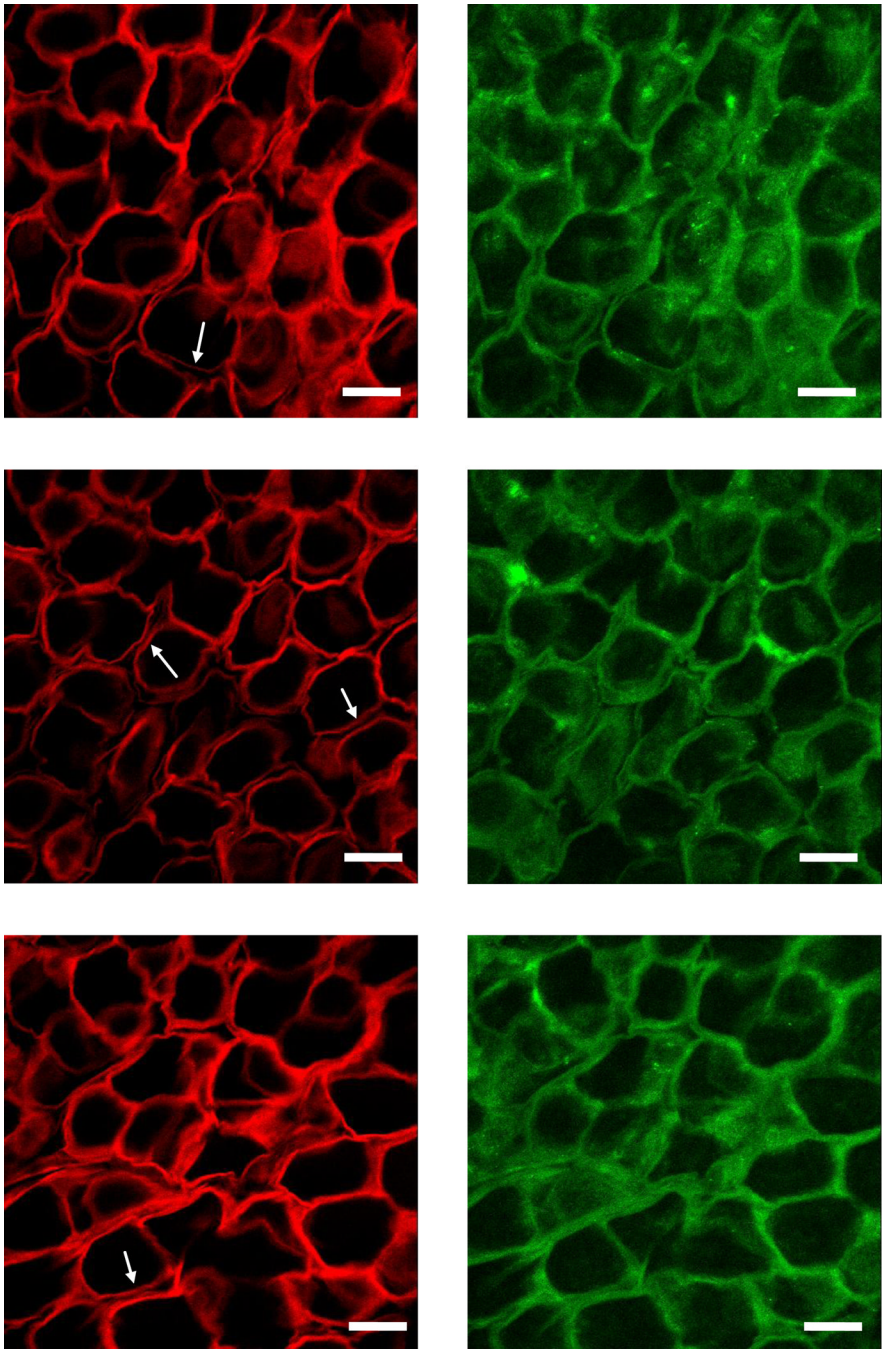

Figure 6.
Representative dual-channel images of SRG and human skin autofluorescence at the skin surface. Left column, SRG channel (the presence of SRG is indicated by the red color); right column, skin autofluorescence channel (the presence of skin fluorophores is indicated by the green color). Arrows point to regions where SRG is only localized within the corneocyte-lipid interface (i.e. SRG is not present throughout the entire intercellular region). Bar = 20 μm.

Table 1

Name and molecular weight (MW) of each of the 12 FPE candidates. Chemical structures are provided in Figure 1.

Acronym	Name	MW (Da)	Structure
AO	acridine orange 10-nonyl bromide	473	1
BODIPY1	BODIPY® 500/510 C_8, C_5	404	2
BODIPY2	BODIPY® FL C_{11}	404	3
DCDHF	2-{3-Cyano-4-[4-(dodecyl-methyl-amino)-phenyl]-5,5-dimethyl-5*H*-furan-2-ylidene}-malononitrile	459	4
FLUOR	5-dodecanoylaminofluorescein	530	5
MO	methyl orange, sodium salt	327	6
RB	rhodamine B chloride	479	7
R6G	rhodamine 6G chloride	479	8
R110	rhodamine 110 chloride	367	9
SRB	sulforhodamine B, sodium salt	581	10
SRG	sulforhodamine G, sodium salt	553	11
TAMRA	5-carboxytetramethylrhodamine	430	12